Two-layer spatial beam with inter-layer slip in longitudinal and transverse direction

G. Udovč, I. Planinc, T. Hozjan, A. Ogrin *

University of Ljubljana, Faculty of Civil and Geodetic Engineering, Jamova cesta 2, 1000 Ljubljana, Slovenia

A B S T R A C T

The paper presents a new mathematical and numerical model for analysis of two-layered spatial beams with inter-layer slip taken into account. Each of the two layers can be made of different material, such as timber, concrete or steel. These layers, connected together, form a composite beam, for example concrete–steel, concrete–timber or timber–timber composite beam. There are several novelties in the presented mathematical and numerical model. The first novelty is that the model enables the analysis of the influence of shear deformations on the stiffness of two-layered spatial beams. The second novelty of the model is that the inter-layer slip can only happen in longitudinal and transverse direction, while inter-layer slip in perpendicular direction is not possible. Yet another important novelty of the model is a consistent separation of the basic equations of the model into two unrelated groups and introduction of appropriate constraining equations. The negative influence of poorly conditioned equations due to the constraint equations, which would otherwise occur during the solving of the equations of the model, is thus avoided. The equations of the presented numerical model are solved by applying the finite elements method. Thus, a new family of deformation based finite elements has been developed, where all the deformation quantities of the beam model are interpolated with Lagrange polynomials of arbitrary degree. By introducing a new deformation based finite element we are able to avoid all types of locking that is typical for displacement-based finite elements. Convergence and parametric studies, presented in the paper, show: (i) that the deformation-based finite elements are very accurate and therefore suitable for the analysis of two-layer spatial beams, (ii) that the inter-layer slip in both considered directions significantly affects the values of physical quantities and therefore has to be considered in the analysis and (iii) that shear deformations have smaller effect on the stiffness of two-layer spatial beams than they have on the stiffness of homogeneous spatial beams.

1. Introduction

Composite elements are used in everyday construction, for example in bridge and high-rise construction, and they are also common in building renovations. They can be found in the form of composite plates or composite beams, mostly with two or three layers joined together, where each layer can be made from different material. By choosing different materials, the designer can take full advantage of their properties, for example concrete can effectively be used in compression, while steel behaves favourably in tension, together forming a strong composite element. The composite behaviour is very dependent on the type of connection between the layers, where mechanical or chemical bonding can be used. Since ideally rigid connection between layers in reality cannot be achieved, some inter-layer slip will always occur. There are several materials, countless configuration possibilities and just as many types of connectors, which can be used in composite

elements. Interesting examples of three layered steel–concrete–steel (SCS) composite beams with mechanical connectors were presented by Liew et al. [1], who more recently published a new, more general, paper with recent innovations of the same type of beam [2]. Similarly, an overview of two layered timber–concrete composite beams was presented by Yeoh et al. [3].

As many studies show, higher contact stiffness results in smaller inter-layer slip [3]. Inter-layer slip significantly affects the stiffness and load-bearing capacity of entire composite beam or plate, as shown for example by Hozjan et al. [4]. Smaller inter-layer slip ensures higher stiffness of the composite element and smaller overall deflections.

In the scientific literature we find numerous researches on models for the analysis of composite beams. Newmark et al. [5], who analysed a two-layered steel–concrete beam, were among the first to research this kind of structures, followed by Goodman and Popov [6,7]. With the development of computers, new numerical and analytical models

for the analysis of composite beams were derived. Many different analytical models considering two-layered composite beams [6,8–10], three or more layered composite beams [11–16], 2-D elastic composite beams [17], Timoshenko two-layered composite beams [18,19], composite beams with considered uplift [20,21], non-linear interface composite beams [22,23], composite columns with buckling [24] and composite beams in dynamics [25] were derived. Similarly many numerical models that describe behaviour of composite structures were also developed. Most of them focused on developing a finite element for two-layered composite beams [4,26–34], others focused on dynamics and vibrations of composite beams [35–37] and some even analysed composite structures in case of fire [38–41]. However, all of the listed researches have one common point and that is that they only made contributions to planar two or more layered composite structures. In scientific literature there is relatively little research on the spatial behaviour of two or more layered composite structures. Challamel and Girhammar [42] were among the first to analyse this kind of structures, followed by Čas et al. [43], where analytical solution of two-layered spatial elastic beam with inter-layer slip in longitudinal and transverse direction was presented. As it is common with analytical solutions, model in [43] is only valid in certain special examples. Spatial composite beam, with inter-layer slip in longitudinal direction and with additionally considered shear deformations, was recently presented by Udovč et al. [44] and was upgraded even further with nonlinear response on the contact by Udovč et al. [45].

In this paper, a new mathematical and numerical model for the analysis of two-layered spatial beams is presented. The novelties are: (i) inter-layer slip is possible in longitudinal and transverse direction and (ii) shear deformations of each layer in both transverse directions are taken into account. Relative displacements between the two layers in direction perpendicular to the contact surface are not included in the model. The model is an upgrade of the research by Čas [27] and Udovč et al. [44]. In research made by Čas [27], a planar composite beam without consideration of shear deformations was presented and only inter-layer slip in longitudinal direction was possible. A research made by Udovč et al. [44] addresses a spatial composite beam with shear deformations already taken into account, however inter-layer slip in that model still occurs only in longitudinal direction.

The generalized equilibrium equations of the new model are derived by linearizing the basic equations of Reissner–Simo theory of spatial beams [46]. By consistently separating equations of the model into two unrelated groups, one can avoid the negative effects of poorly conditioned equations due to the constraining equations, which is also one of the advantages of this model over numerical models implemented in various commercial software. In order to solve the system of equations, a finite element method is used, where a new family of deformation based finite elements is derived.

In deformation based finite elements one interpolates deformational quantities (axial, shear, bending and torsional deformations), which means that the deformations are the unknowns we are looking for [47]. There are many other different formulation approaches, such as displacement based approach [48], force based approach [49,50], velocity based approach [51] and mixed approach [52,53], which consist of two or more different approaches combined together. Every approach has its own weaknesses and benefits. The main advantage of deformation based finite elements is the absence of locking, which can sometimes occur with displacement based finite elements [27,49,54,55]. By using deformations as interpolation functions the constitutive equations are perfectly satisfied. Since the equality of equilibrium and constitutive forces is demanded in the model, the oscillation of internal forces, which causes locking, is prevented. The benefit of deformation based finite elements was also presented by Choi et al. [56].

In the paper, generalized equilibrium equations of the beam are presented first, followed by a presentation of numerical solving and finally multiple parametric studies are shown. This model is relatively simple and the presented numerical example could have just as well

been analysed with some commercial software using solid finite elements. However, it is important to emphasize that there are several scientific fields, where the novel model with its advantages can be applied as a foundation for further research. For example, it could be upgraded for analysis of spatial composite beams with material and contact nonlinearity, for analysis of influence of transverse slip on the warping deformations or for analysis of spatial composite beams in fire conditions.

2. Basic equations

This section contains assumptions, basic equations of each separate homogeneous layer, constraining equations, which connect layers together, and finally generalized equilibrium equations of a two-layer spatial beam.

2.1. Assumptions

A two-layer spatial beam made of lower layer a and upper layer b is considered. The assumptions, which apply in the presented mathematical model of the two-layer spatial beam, are divided into three categories: geometrical assumptions determine shape and size of the beam and belong to the first category, assumptions about the contact between the layers are gathered in the second category, and last category of assumptions describes material properties of both layers.

A. Assumptions about geometry of the beam.

- Changes in shape and size of each layer due to the external loads are small and therefore a linear theory of spatial beams is taken into account.
- The reference axis of each layer passes through the cross-sectional centroid of that layer. The two reference axes are straight and parallel to each other in undeformed placement.
- The shape and size of each layers cross-section are arbitrary, however they are constant along the length of the beam and they do not change during deformation.
- The cross-sections of each layer are planar in undeformed placement and perpendicular to the reference axes and they remain plane after deformation. However, they are no longer perpendicular to the reference axis corresponding. The later enables consideration of shear deformations of the beam.

B. Assumptions about the contact.

- Inter-layer slip in both longitudinal and transverse direction is possible.
- The contact is rigid in the direction perpendicular to the contact surface.
- Inter-layer slip in longitudinal and transverse direction is small, therefore linearized constraint equations are taken into account. This assumption is justified since inter-layer slip in everyday composite structures is very small.
- Rotations of the cross-sections are equal for both layers.

C. Assumptions about materials.

- Material model of each layer of the beam is linear elastic in accordance with Hooke's law.
- Material properties of each layer can be different.
- Material model of the contact is linear elastic. Inter-layer slip is therefore directly proportional to contact stiffness. Equations for longitudinal and transverse inter-layer slip are independent from each other.

An undeformed and a deformed placement of the two-layer beam, in accordance with assumptions about geometry, are presented in Fig. 1. The deformation of the beam is described in a three-dimensional Euclidean space denoted by $\mathcal{E}$. The coordinates of the global Cartesian
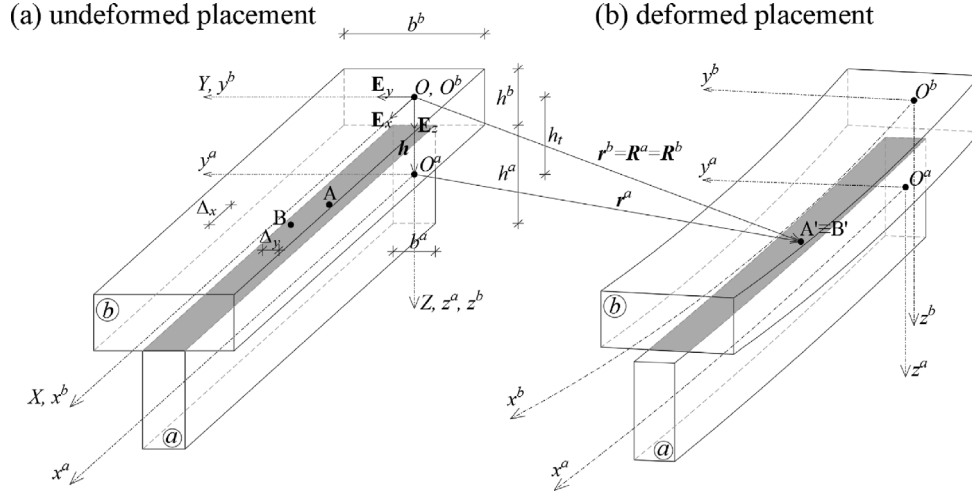
(a) undeformed placement   (b) deformed placement

Fig. 1. Two-layer spatial beam (a) in undeformed placement and (b) in deformed placement.

coordinate system in $\mathcal{E}$ are denoted by X, Y and Z. The corresponding base vectors of the described global coordinate system are $\boldsymbol{E}_x$, $\boldsymbol{E}_y$, $\boldsymbol{E}_z$, where $\boldsymbol{E}_z = \boldsymbol{E}_x \times \boldsymbol{E}_y$. The observation point of the global coordinate system is chosen at $O = (0,0,0)$ from where a position vector $\boldsymbol{R}$ determines any point in $\mathcal{E}$. Each layer has a local coordinate system, which is, in undeformed placement, also Cartesian. Local coordinates of each layer i are denoted by x^i, y^i and z^i, while the corresponding local base vectors of each layer are denoted by $\boldsymbol{e}_x^i$, $\boldsymbol{e}_y^i$, $\boldsymbol{e}_z^i$, where $\boldsymbol{e}_z^i = \boldsymbol{e}_x^i \times \boldsymbol{e}_y^i$ and $i = a, b$. The observation point of local coordinate system for layer b (O^b) is at the same point as the observation point of the global coordinate system (O), while the observation point of local coordinate system for layer a is $h_t \boldsymbol{E}_z$ away from observation point O. The axes of the global and local coordinate systems are shown in Fig. 1. In the deformed placement, the local coordinate system of each layer is chosen such that the local coordinates of each point in the undeformed and deformed placement are the same. The local coordinate system chosen in this way is curvilinear and the coordinates are called convective coordinates.

Deformed placement of layer a and b in $\mathcal{E}$ is described with a position vector $\boldsymbol{R}^i$, where $i = a, b$. In global coordinate system vector $\boldsymbol{R}^i$ can be expressed as $\boldsymbol{R}^i = X^i \boldsymbol{E}_x + Y^i \boldsymbol{E}_y + Z^i \boldsymbol{E}_z$. Another way of expressing vector $\boldsymbol{R}^i$ is with local coordinates using local vectors $\boldsymbol{r}^i$ as shown in Eqs. (1) and (2).

$$\begin{aligned} \boldsymbol{R}^a &= h_t \boldsymbol{E}_z + \boldsymbol{r}^a, \\ \boldsymbol{R}^b &= \boldsymbol{r}^b. \end{aligned} \tag{1}$$

$$\begin{aligned} \boldsymbol{r}^i &= x^i \boldsymbol{e}_x^i + y^i \boldsymbol{e}_y^i + z^i \boldsymbol{e}_z^i + \boldsymbol{u}^i + \boldsymbol{\varphi}^i \times \boldsymbol{\rho}^i, \\ \boldsymbol{u}^i &= u^i \boldsymbol{e}_x^i + v^i \boldsymbol{e}_y^i + w^i \boldsymbol{e}_z^i, \\ \boldsymbol{\rho}^i &= y^i \boldsymbol{e}_y^i + z^i \boldsymbol{e}_z^i, \\ \boldsymbol{\varphi}^i &= \varphi_x^i \boldsymbol{e}_x^i + \varphi_y^i \boldsymbol{e}_y^i + \varphi_z^i \boldsymbol{e}_z^i. \end{aligned} \tag{2}$$

By using Eqs. (1) and (2) one can express deformed placement of each layer a and b, where vectors $\boldsymbol{u}^i$ and $\boldsymbol{\varphi}^i$ are dependent on x^i of each layer.

2.2. Basic equations of homogeneous layer

Basic equations of each homogeneous layer of the beam are well known, thus they are summarized here, based on the literature [57]. They consist of kinematic, equilibrium and constitutive equations with corresponding static and kinematics boundary conditions for each layer $i = a, b$.

$$\begin{aligned} \varepsilon_x^i - u^{i\prime} &= 0, \\ \gamma_y^i - v^{i\prime} + \varphi_z^i &= 0, \\ \gamma_z^i - w^{i\prime} - \varphi_y^i &= 0, \\ \kappa_x^i - \varphi_x^{i\,\prime} &= 0, \\ \kappa_y^i - \varphi_y^{i\,\prime} &= 0, \\ \kappa_z^i - \varphi_z^{i\,\prime} &= 0. \end{aligned} \tag{3}$$

$$\begin{aligned} N_x^{i\prime} + p_x^i &= 0, \\ N_y^{i\prime} + p_y^i &= 0, \\ N_z^{i\prime} + p_z^i &= 0, \\ M_x^{i\prime} + m_x^i &= 0, \\ M_y^{i\prime} - N_z^i + m_y^i &= 0, \\ M_z^{i\prime} + N_y^i + m_z^i &= 0. \end{aligned} \tag{4}$$

$$\begin{aligned} N_x^i - N_{x,c}^i &= N_x^i - E^i A_x^i \varepsilon_x^i = 0, \\ N_y^i - N_{y,c}^i &= N_y^i - G^i A_s^i \gamma_y^i = 0, \\ N_z^i - N_{z,c}^i &= N_z^i - G^i A_s^i \gamma_z^i = 0, \\ M_x^i - M_{x,c}^i &= M_x^i - G^i I_t^i \kappa_x^i = 0, \\ M_y^i - M_{y,c}^i &= M_y^i - E^i I_y^i \kappa_y^i - E^i I_{yz}^i \kappa_z^i = 0, \\ M_z^i - M_{z,c}^i &= M_z^i - E^i I_{yz}^i \kappa_y^i - E^i I_z^i \kappa_z^i = 0. \end{aligned} \tag{5}$$

In Eqs. (3)–(5), u^i, v^i and w^i represent displacements of the reference axis of each layer in x, y and z direction, while φ_x^i, φ_y^i and φ_z^i represent rotations of the reference axis of each layer. Deformations are denoted by ε_x^i, γ_y^i, γ_z^i, κ_x^i, κ_y^i and κ_z^i, where ε_x^i represents axial deformation, γ_y^i and γ_z^i represent shear deformations in y and z direction, respectively, κ_x^i represents torsional deformation and κ_y^i and κ_z^i represent bending deformations around y and z axis of each layer. With N_x^i, N_y^i, N_z^i, M_x^i, M_y^i and M_z^i a well known internal forces and moments for each layer are denoted, while $N_{x,c}^i$, $N_{y,c}^i$, $N_{z,c}^i$, $M_{x,c}^i$, $M_{y,c}^i$ and $M_{z,c}^i$ denote the corresponding constitutional forces and moments for each layer according to Hooke's law. External line loads for each layer are denoted with p_x^i, p_y^i, p_z^i, m_x^i, m_y^i and m_z^i, where each component consists of actual external load and of contact stresses between layers a and b. Eqs. (5) contain material and geometrical properties of each layer. E^i and G^i represent Young's and shear modulus for each layer a and b. Area of

cross-section for each layer is denoted by A_x^i, while moments of inertia for each layer are denoted by I_y^i, I_z^i and I_{yz}^i. It is well known that shear and torsional stiffness are overestimated within applied material models, since bulging of cross-sections is not considered. In order to mitigate this disadvantage, the so-called shear cross-sections A_s^i of each layer and torsional moments of inertia I_t^i for each layer are considered, as proposed by Cowper [58] and Hjelmstad [57].

2.3. Constraining equations

Behaviour of a two-layer spatial beam is very dependant on type of connection used for connecting layers together. A completely rigid connection between layers is practically impossible to ensure, consequently, an inter-layer slip occurs. In the presented theory, only inter-layer slip in longitudinal and transverse direction is possible, where contact behaviour is linear with a prescribed stiffness in each direction.

2.3.1. Kinematic constraining equations

The kinematic constraining equations of the two-layer spatial beam are derived by the requirement that particles A and B on the contact surface, which are at different positions in undeformed placement, join together in particle A'≡B' in deformed placement. Point A and A' represent a particle on layer a, while point B and B' represent a particle on layer b. This requirement can be described with vectors, where one takes into account that deformed placement of contact point A is dependant on coordinates $(x, y, -\frac{h^a}{2})$ and deformed placement of contact point B is dependant on coordinates $(x^*, y^*, \frac{h^b}{2})$, as shown in Eq. (6).

$$\mathbf{r}^a(x, y, -\frac{h^a}{2}) = \mathbf{r}^b(x^*, y^*, \frac{h^b}{2}) - \mathbf{h}. \tag{6}$$

One of the basic assumptions is that displacements and rotations of cross-sections are small and consequently inter-layer slip between layers will also be small. Thus, it makes sense to replace the non-linear constraint presented in Eq. (6) with linear ones, which are determined by linearization of the Eq. (6) around the initial undeformed placement of the beam. After a short calculus, three linearized kinematic constraining equations are obtained, to which additional three kinematic constraining equations for rotations of the layers are added in accordance with the assumptions, as shown in Eqs. (7) and (8).

$$x + u^a = x^* + u^b + h_t \varphi_y,$$
$$y + v^a = y^* + v^b - h_t \varphi_x,$$
$$w^a = w^b = w. \tag{7}$$

$$\varphi_x^a = \varphi_x^b = \varphi_x,$$
$$\varphi_y^a = \varphi_y^b = \varphi_y,$$
$$\varphi_z^a = \varphi_z^b = \varphi_z. \tag{8}$$

Finally, the inter-layer slip vector $\mathbf{\Delta} = \Delta_x \mathbf{E}_x + \Delta_y \mathbf{E}_y + \Delta_z \mathbf{E}_z$ is introduced, since it will be needed for the formulation of constitutive constraining equations.

$$\Delta_x = x - x^* = u^b - u^a + h_t \varphi_y,$$
$$\Delta_y = y - y^* = v^b - v^a - h_t \varphi_x, \tag{9}$$
$$\Delta_z = 0.$$

Inter-layer slip vector can be defined as

$$\mathbf{\Delta} = \mathbf{r}^b(x, y, \frac{h^b}{2}) - \mathbf{h} - \mathbf{r}^a(x, y, -\frac{h^a}{2}). \tag{10}$$

Note, that $\mathbf{r}^a$ and $\mathbf{r}^b$ in Eq. (10) depend on the same x and y coordinates.

2.3.2. Deformation constraining equations

By combining kinematic constraining Eqs. (7) and (8) and kinematic equations of homogeneous layer (Eqs. (3)), one can derive deformation constraining Eqs. (11)

$$1 + \varepsilon_x^a - h_t \kappa_y = x^{*\prime} + \varepsilon_x^b,$$
$$\gamma_y^a + h_t \kappa_x = y^{*\prime} + \gamma_y^b,$$
$$\gamma_z^a = \gamma_z^b = \gamma_z,$$
$$\kappa_x^a = \kappa_x^b = \kappa_x, \tag{11}$$
$$\kappa_y^a = \kappa_y^b = \kappa_y,$$
$$\kappa_z^a = \kappa_z^b = \kappa_z.$$

2.3.3. Constitutive constraining equations

Material properties of the contact are introduced into the system of equations through the constitutive constraining equations. Since, in the presented theory, only longitudinal and transverse inter-layer slip between layers $i = a, b$ are possible, equilibrium surface contact loads for the two directions, x and y, are defined as q_x^i and q_y^i. The following equalities are assumed: $q_x^a = -q_x^b = q_x = q_{x,c}$ and $q_y^a = -q_y^b = q_y = q_{y,c}$, where $q_{x,c}$ and $q_{y,c}$ represent constitutive surface contact loads. As described in Section 2.2, the external line loads p_x^i, p_y^i, p_z^i, m_x^i, m_y^i and m_z^i consist of actual external line loads and contact line loads. In Eqs. (12) $(\bullet)_{j,e}^i$ represents actual external line loads and $(\bullet)_{j,c}^i$ represents contact line loads, where $j = x, y, z$.

$$p_j^i = p_{j,e}^i + p_{j,c}^i,$$
$$m_j^i = m_{j,e}^i + m_{j,c}^i. \tag{12}$$

The actual external line loads $(\bullet)_{j,e}^i$ are input data and do not require further explanations, whereas contact line loads $(\bullet)_{j,c}^i$ do. Contact line loads are obtained by integrating equilibrium surface contact loads as shown in Eqs. (13), where $j = x, y, z$.

$$p_{j,c}^a = -p_{j,c}^b = \int_0^{b_c} q_j \, dy,$$
$$m_{x,c}^i = \int_0^{b_c} (y^i q_z^i - z^i q_y^i) \, dy,$$
$$m_{y,c}^i = \int_0^{b_c} (z^i q_x^i) \, dy, \tag{13}$$
$$m_{z,c}^i = -\int_0^{b_c} (y^i q_x^i) \, dy.$$

In the presented theory, the contact behaviour is linear and, since inter-layer slip is only possible in longitudinal and transverse direction, only $q_{x,c}$ and $q_{y,c}$ need to be defined. The simplest linear elastic relation is considered, as shown in Eqs. (14).

$$p_{x,c}^a = -p_{x,c}^b = \int_0^{b_c} q_{x,c} \, dy = b_c k_x \Delta_x = K_x \Delta_x,$$
$$p_{y,c}^a = -p_{y,c}^b = \int_0^{b_c} q_{y,c} \, dy = b_c k_y \Delta_y = K_y \Delta_y, \tag{14}$$

where k_x and k_y represent surface stiffness of the contact, while K_x and K_y represent surface stiffness of the contact multiplied by width of the contact surface b_c. Stiffness depends on the type of connection that is used between both layers.

As already mentioned above, the only parameter that defines the behaviour on the contact in this model is contact stiffness of shear connection between layers. The contact stiffness thus includes all aspects of the connection, such as type of connectors, their geometry, spacing between connectors, friction between contact surface, *etc.* Behaviour of shear connections (e.g. shear studs or adhesive in glued joints) is typically determined with shear tests and its results are described through force-slip diagram. For higher loads, the force-slip relationship is usually nonlinear [3]. For smaller loads, however, the diagram is linear and a simple correlation between contact load q_c and slip Δ can be obtained, gaining contact stiffness $K = q_c/\Delta$. For the level of loads, that

typically occur in general use of composite structures, the behaviour on the contact is mostly linear and thus the assumption of linear behaviour on the contact in this model is justified. For higher loads and cases where composite structures are exposed to fire, properties of connectors and also of each layer become nonlinear and therefore a linear contact stiffness is not realistic nor a suitable assumption. The influence of non-linear contact behaviour in case of room temperature and in case of fire, where Nelson shear studs are used, was presented by Huang et al. [59].

2.4. Generalized equilibrium equations of two-layer spatial beam

The generalized equilibrium equations of the two-layer spatial beam are derived by using basic Eqs. (3)–(5) for each homogeneous layer $i = a, b$ and constraining Eqs. (7) and (8). Generalized equilibrium equations, which are not to be confused with equilibrium equations, consist of equilibrium, kinematic and constitutive equations as shown in Eqs. (15)–(17) and corresponding kinematic and static boundary conditions as shown in Eqs. (18) and (19), where $i = a, b$, $j = x, y, z$ and $k = 0, L$.

$$N_x^{i\,\prime\prime} + p_{x,e}^i + p_{x,c}^i = 0,$$
$$N_y^{i\,\prime\prime} + p_{y,e}^i + p_{y,c}^i = 0,$$
$$N_z^{\prime} + p_{z,e}^a + p_{z,c}^b = 0,$$
$$M_x^{\prime} + m_{x,e}^a + m_{x,e}^b + h_t p_{y,c}^a = 0, \tag{15}$$
$$M_y^{\prime} - N_z + m_{y,e}^a + m_{y,e}^b - h_t p_{x,c}^a = 0,$$
$$M_z^{\prime} + N_y^a + N_y^b + m_{z,e}^a + m_{z,e}^b = 0.$$

$$\varepsilon_x^i - u^{i\,\prime\prime} = 0,$$
$$\gamma_y^i - v^{i\,\prime} + \varphi_z = 0,$$
$$\gamma_z - w^{\prime} - \varphi_y = 0, \tag{16}$$
$$\kappa_j - \varphi_j^{\,\prime} = 0.$$

$$N_{x,c}^i - E^i A_x^i \varepsilon_x^i = 0,$$
$$N_{y,c}^i - G^i A_s^i \gamma_y^i = 0,$$
$$N_{z,c} - (G^a A_s^a + G^b A_s^b)\gamma_z = 0,$$
$$M_{x,c} - (G^a I_t^a + G^b I_t^b)\kappa_x = 0, \tag{17}$$
$$M_{y,c} - (E^a I_y^a + E^b I_y^b)\kappa_y - (E^a I_{yz}^a + E^b I_{yz}^b)\kappa_z = 0,$$
$$M_{z,c} - (E^a I_z^a + E^b I_z^b)\kappa_z - (E^a I_{yz}^a + E^b I_{yz}^b)\kappa_y = 0.$$

$$u^i(k) = u_k^i,$$
$$v^i(k) = v_k^i,$$
$$w(k) = w_k, \tag{18}$$
$$\varphi_y^i(k) = \varphi_{j,k}^i.$$

$$N_j^i(k) = N_{j,k}^i,$$
$$N_z(k) = N_{z,k}, \tag{19}$$
$$M_j(k) = M_{j,k}.$$

Eqs. (15)–(17), together with boundary conditions from Eqs. (18) and (19) represent the 1st group of basic equations of the model. After the 1st group of basic equations is solved, the 2nd group can easily be derived, since equations there are dependant on the values from the 1st group. By solving basic equations of the 2nd group, which are not presented here, one can obtain values of typical static and kinematic quantities, such as γ_z^b, κ_x^b, κ_y^b, κ_z^b, N_z^a, M_x^a, M_y^a, M_z^a, N_z^b, M_x^b, M_y^b, M_z^b, w^b, φ_x^b, φ_y^b and φ_z^b. System of equations presented in this section is linear elastic and can be upgraded with material nonlinearity of each layer and nonlinear behaviour on the contact between layers. This can be achieved by changing Eqs. (14) and (17) into functions of stresses. In order to implement geometrical nonlinearity into the system of equations, a completely new derivation of system of equations would be needed due to the nonlinearity in kinematic equations.

3. Numerical implementation

3.1. Modified virtual work

The generalized equilibrium equations of the two-layer spatial beam presented in Eqs. (15)–(17), together with corresponding kinematic and static boundary conditions presented in Eqs. (18) and (19) are solved numerically. A new family of deformation based spatial two-layer beam finite elements, which is presented hereinafter, is applied. The new family is similar to the family of planar two-layer beam finite elements already presented by Čas [27]. Generalized equilibrium equations can successfully be solved if deformations, as well as all of the 16 constants of integration ($u^a(0)$, $u^b(0)$, $v^a(0)$, $v^b(0)$, $w(0)$, $\varphi_x(0)$, $\varphi_y(0)$, $\varphi_z(0)$, $N_x^a(0)$, $N_x^b(0)$, $N_y^a(0)$, $N_y^b(0)$, $N_z(0)$, $M_x(0)$, $M_y(0)$ and $M_z(0)$) are known.

With the help of constitutive equations, one can express deformations as functions of internal static quantities. According to the deformation based finite element method, the constitutive equations must be expressed in the form of a functional, *i.e.* in the form of a modified virtual work [27]. By observing virtual work of two-layer spatial beam with corresponding kinematic equations, which represent constraining equations to the functional, modified virtual work can be derived. In accordance with the method of Lagrange multipliers, the kinematic equations are multiplied by arbitrary functions, then they are varied and, finally, added to the virtual work. The obtained modified virtual work is:

$$\delta W^* = \int_0^L [(N_{x,c}^a - N_x^a)\delta\varepsilon_x^a + (N_{x,c}^b - N_x^b)\delta\varepsilon_x^b + (N_{y,c}^a - N_y^a)\delta\gamma_y^a +$$
$$+ (N_{y,c}^b - N_y^b)\delta\gamma_y^b + (N_{z,c} - N_z)\delta\gamma_z + (M_{x,c} - M_x)\delta\kappa_x + \tag{20}$$
$$+ (M_{y,c} - M_y)\delta\kappa_y + (M_{z,c} - M_z)\delta\kappa_z] \, \mathrm{d}\xi.$$

Kinematic and static boundary conditions, which are presented in Eqs. (18) and (19), represent constraining equations to the modified virtual work (Eq. (20)).

3.2. Numerical analysis

Modified virtual work, together with static and kinematic boundary conditions (Eqs. (18) and (19)), is used for final derivation of the deformation based finite element for the analysis of two-layer spatial beams. A beam is divided into n_{FE} number of finite elements with a length L_{FE}. $n_N = n_{FE+1}$ denotes the number of nodes and n_B is the number of kinematic boundary conditions, *i.e.*, number of degrees of freedom restrained by supports. Gauss quadrature rule for numerical integration is used, where n represents the number of integration points in one finite element. Lagrange interpolation polynomials of degree $n-1$, which are denoted by $P_i(x)$ for $i = 1, 2, \ldots, n$, are applied for the interpolation. When each deformation is written as $(\bullet)(x) = \sum_{i=1}^n P_i(x)(\bullet)_i$ and each inherent variation is written as $\delta(\bullet)(x) = \sum_{i=1}^n P_i(x)\delta(\bullet)_i$, they are inserted into modified virtual work, and the following system of equations for each finite element is obtained:

$$g_i = \int_0^{L_{FE}} (N_{x,c}^a - N_x^a)P_i \mathrm{d}\xi = 0,$$

$$g_{i+n} = \int_0^{L_{FE}} (N_{x,c}^b - N_x^b)P_i \mathrm{d}\xi = 0,$$

$$g_{i+2n} = \int_0^{L_{FE}} (N_{y,c}^a - N_y^a)P_i \mathrm{d}\xi = 0,$$

$$g_{i+3n} = \int_0^{L_{FE}} (N_{y,c}^b - N_y^b)P_i \mathrm{d}\xi = 0,$$

$$g_{i+4n} = \int_0^{L_{FE}} (N_{z,c} - N_z)P_i \mathrm{d}\xi = 0, \tag{21}$$

$$g_{i+5n} = \int_0^{L_{FE}} (M_{x,c} - M_x)P_i \mathrm{d}\xi = 0,$$

$$g_{i+6n} = \int_0^{L_{FE}} (M_{y,c} - M_y)P_i \mathrm{d}\xi = 0,$$

$$g_{i+7n} = \int_0^{L_{FE}} (M_{z,c} - M_z)P_i \mathrm{d}\xi = 0.$$

$$g_{8n+1} = u^a(L_{FE}) - u^a(0) - \sum_{i=1}^{n} \int_0^{L_{FE}} P_i \varepsilon_{x,i}^a \,d\xi = 0,$$

$$g_{8n+2} = u^b(L_{FE}) - u^b(0) - \sum_{i=1}^{n} \int_0^{L_{FE}} P_i \varepsilon_{x,i}^b \,d\xi = 0,$$

$$g_{8n+3} = v^a(L_{FE}) - v^a(0) - \sum_{i=1}^{n} \int_0^{L_{FE}} P_i \gamma_{y,i}^a \,d\xi -$$
$$- \varphi_z(0)L_{FE} - \sum_{i=1}^{n} \int_0^{L_{FE}} \int_0^{x} P_i \kappa_{z,i} \,d\xi \,d\xi = 0,$$

$$g_{8n+4} = v^b(L_{FE}) - v^b(0) - \sum_{i=1}^{n} \int_0^{L_{FE}} P_i \gamma_{y,i}^b \,d\xi -$$
$$- \varphi_z(0)L_{FE} - \sum_{i=1}^{n} \int_0^{L_{FE}} \int_0^{x} P_i \kappa_{z,i} \,d\xi \,d\xi = 0,$$

(22)

$$g_{8n+5} = w(L_{FE}) - w(0) - \sum_{i=1}^{n} \int_0^{L_{FE}} P_i \gamma_{z,i} \,d\xi +$$
$$+ \varphi_y(0)L_{FE} + \sum_{i=1}^{n} \int_0^{L_{FE}} \int_0^{x} P_i \kappa_{y,i} \,d\xi \,d\xi = 0,$$

$$g_{8n+6} = \varphi_x(L_{FE}) - \varphi_x(0) - \sum_{i=1}^{n} \int_0^{L_{FE}} P_i \kappa_{x,i} \,d\xi = 0,$$

$$g_{8n+7} = \varphi_y(L_{FE}) - \varphi_y(0) - \sum_{i=1}^{n} \int_0^{L_{FE}} P_i \kappa_{y,i} \,d\xi = 0,$$

$$g_{8n+8} = \varphi_z(L_{FE}) - \varphi_z(0) - \sum_{i=1}^{n} \int_0^{L_{FE}} P_i \kappa_{z,i} \,d\xi = 0.$$

$$-N_x^a(L_{FE-1}) + N_x^a(L_{FE}) + S_1 = 0,$$
$$-N_x^b(L_{FE-1}) + N_x^b(L_{FE}) + S_2 = 0,$$
$$-N_y^a(L_{FE-1}) + N_y^a(L_{FE}) + S_3 = 0,$$
$$-N_y^b(L_{FE-1}) + N_y^b(L_{FE}) + S_4 = 0,$$
$$-N_z(L_{FE-1}) + N_z(L_{FE}) + S_5 = 0,$$
$$-M_x(L_{FE-1}) + M_x(L_{FE}) + S_6 = 0,$$
$$-M_y(L_{FE-1}) + M_y(L_{FE}) + S_7 = 0,$$
$$-M_z(L_{FE-1}) + M_z(L_{FE}) + S_8 = 0.$$

(23)

In Eqs. (21) and (22), i represents each interpolation point inside a finite element. System of Eqs. (21) has $8n$ equations for determining $8n$ unknown deformation quantities ($\varepsilon_{x,i}^a, \varepsilon_{x,i}^b, \gamma_{y,i}^a, \gamma_{y,i}^b, \gamma_{z,i}, \kappa_{x,i}, \kappa_{y,i}$ and $\kappa_{z,i}$) for each finite element. With Eqs. (22) the prescribed kinematic boundary conditions in each finite element are satisfied, consequently connecting finite elements into a beam, where there are $8n_N - n_B$ unknown kinematic quantities for 8 equations for each finite element. The final system of Eqs. (23) ensures equilibrium at all nodes of the finite element mesh, thus gaining $8n_N - n_B$ equations for 8 unknowns in each finite element, where S_i represents external generalized point forces in the nodes. System of Eqs. (21)–(23) consist of $(8n + 8 + 8n_N - n_B)n_{FE}$ equations for the same amount of unknowns and, therefore, it is solvable. The unknowns are deformations at all interpolation points of the finite elements, the generalized displacements and rotations at the start and the end nodes of each finite element and values of the generalized internal static quantities at the beginning of each finite element.

System of Eqs. (21)–(23) is linear, but can be upgraded with material nonlinearity of each layer and nonlinear behaviour on the contact between layers. When adding material nonlinearity of each layer and nonlinear behaviour on the contact to the system, only constitutive parts in equations would change and everything else would stay the same. Analysis of composite beams exposed to elevated and varying temperatures would require changes in constitutive equations because of temperature dependent material models. It would also require inclusion of other phenomena related to elevated temperature, such as thermal elongation, viscous creep (steel), moisture transfer (concrete,

Table 1
Material properties of each layer.

	E^i [kN/cm^2]	G^i [kN/cm^2]	ρ^i [kg/m^3]
layer a	1200	75	460
layer b	950	59	400

Table 2
Static and kinematic boundary conditions.

$x = 0$ (point A)		$x = L/2$ (point B)		$x = L$ (point C)	
$u^a = 0$	$u^b = 0$	$v^a = 0$	$v^b = 0$	$u^a = 0$	$u^b = 0$
$v^a = 0$	$v^b = 0$	$w = 0$	$\varphi_x = 0$	$v^a = 0$	$v^b = 0$
$w = 0$	$\varphi_x = 0$			$w = 0$	$\varphi_x = 0$
$M_y = 0$	$M_z = 0$			$M_y = 0$	$M_z = 0$

Table 3
Geometrical properties of each layer.

	A_x^i [cm^2]	A_s^i [cm^2]	I_t^i [cm^4]	I_y^i [cm^4]	I_z^i [cm^4]
layer a	450	375	23 186.25	33 750	8437.5
layer b	400	333.33	11 240	3333.33	53 333.33

wood), charring (wood), *etc.* When adding geometrical nonlinearity to the system, the whole set of equations would change and another derivation would be needed, since kinematic equations would be different.

4. Illustrative example

A two-layer, two-span continuous beam, made of timber, with a total length L has been chosen for an illustrative example as shown in Fig. 2. The lower layer is referred to as layer a and the upper layer as layer b. The cross section dimensions of layer a are $b^a/h^a = 15/30$ cm, whereas the cross section dimensions of layer b are $b^b/h^b = 40/10$ cm. The vertical distance between centroids of each layer is $h_t = h^a/2 + h^b/2$. Both of the layers are made of timber; layer a belongs to C30 and layer b belongs to C20 strength class, according to EN 1995-1-1:2005 [60]. Material properties of each layer, such as elasticity modulus E^i, shear modulus G^i and density ρ^i are taken in accordance with the standard EN 1995-1-1:2005 [60] and are presented in Table 1. Supports A, B and C are located at $x = 0$, $x = L/2$ and $x = L$, respectively. The static and kinematic boundary conditions of each support are presented in Table 2. Beam is loaded with three different external line loads which act only on layer b, while layer a is not loaded. The external loads are named $p_{z,e1}^b$, $p_{z,e2}^b$ and $p_{y,e}^b$ and are shown in Fig. 2. While $p_{y,e}^b$ acts at the reference axis of layer b, the remaining two loads act on the upper left and right edges of layer b. Their values are $p_{z,e1}^b = 5$ kN/m, $p_{z,e2}^b = 10$ kN/m and $p_{y,e}^b = 2$ kN/m. Layer a and b are connected together through mechanical or chemical bonding agents, where linear behaviour on the contact, with a contact stiffness in both longitudinal and transverse direction $K_x = K_y$, is assumed.

Geometrical properties of each layer are presented in Table 3. According to Cowper [58] and Hjelmstad [57], shear cross section of each layer, A_s^i, has been multiplied by 5/6 and torsional moments of inertia have been calculated as shown in Eqs. (24).

$$I_t^a = 0.229 h^a b^{a3}$$
$$I_t^b = 0.281 b^b h^{b3}$$

(24)

4.1. Convergence study

Convergence study of deformation based finite elements for the analysis of two-layer planar beams with inter-layer slip has already been presented by Čas [27] and Hozjan [4]. This paper presents a new deformation based finite element for spatial analysis of similar beams, thus a new convergence study is necessary in order to prove
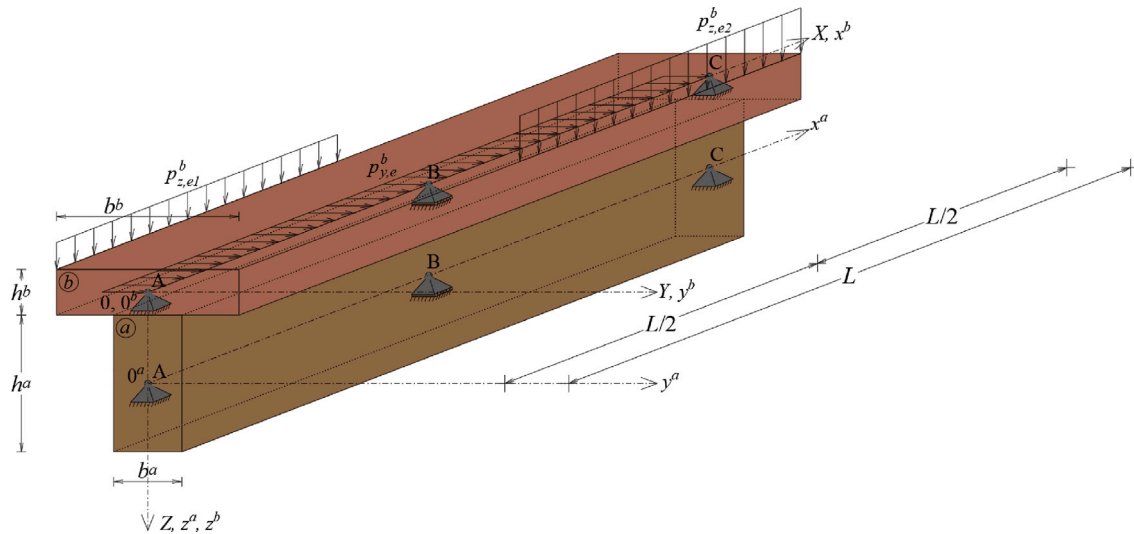
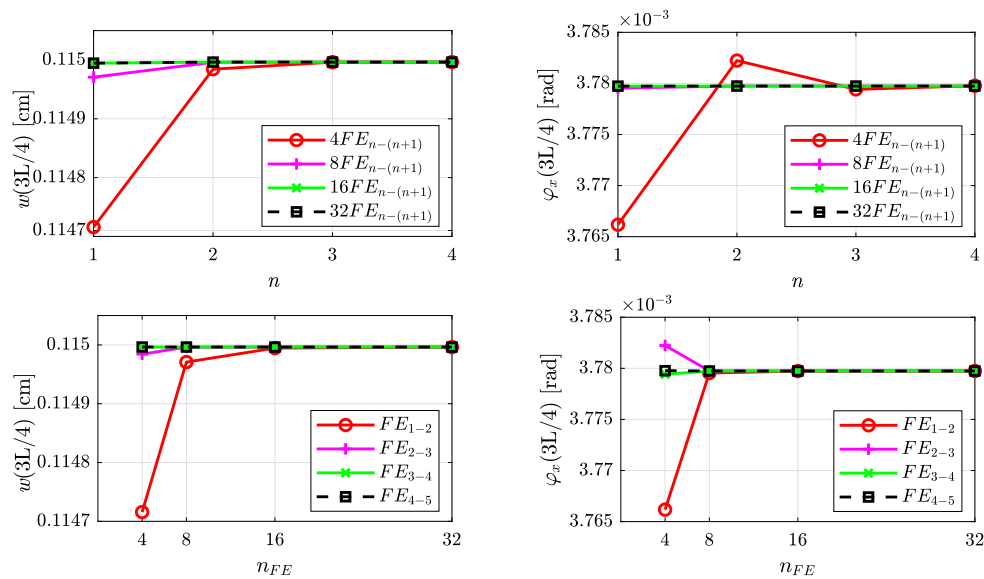**Fig. 2.** Two-layer beam made of timber.

Fig. 3. Convergence study of analysed beam.

adequacy of the element. Speciality of deformation based finite element is that one interpolates deformations instead of displacements. By doing that, all kinds of locking, which are typical for displacements based finite element, are avoided [27]. The beam consists of n_{FE} number of finite elements, where deformations are interpolated by using Lagrange interpolating polynomial of n-degree and integrals are solved by using m-point Gaussian quadrature rule for numerical integration. It is well known that for Lagrange interpolating polynomial of n-degree, one should use $n+1$-point Gaussian quadrature rule for integration, in order to achieve the most optimal performance of finite element [61]. For the purpose of this convergence study the finite element is denoted as FE_{n-m}. A beam with a length $L = 600$ cm and a contact stiffness $K_x = K_y = 10$ kN/cm is chosen. The following Fig. 3 presents results of a convergence study of a beam, described in illustrative example, where the number of finite elements n_{FE} varies as well as a degree of Lagrange polynomial n. As mentioned above, a $(n+1)$-point Gaussian quadrature rule is applied for integration. In convergence study a vertical deflection w and torsional rotation φ_x at $x = 3L/4$ are observed.

It can be seen from Fig. 3, that the convergence obtained with this type of finite element is very good. Results, obtained with 16 finite

elements of type FE_{4-5}, are here regarded as the reference values. Almost exact values of typical physical quantities can be obtained just by using 4 finite elements (*i.e.*, just 2 finite elements per span) with Lagrange polynomial of 3rd degree or by using 16 finite elements with Lagrange polynomial of 1st degree. Hereinafter, 16 finite elements of type FE_{4-5} are used, since calculation time remains very short regardless of the increased n and m, which is due to the linearity of the equations.

4.2. Parametric study of the effect of cross-sectional shear stiffness

In this subsection an influence of cross-sectional shear stiffness on typical kinematic quantities of the beam is presented on an example of two beams, with different length L. Contact stiffness in both longitudinal and transverse direction for both beams is $K_x = K_y = 10$ kN/cm. The length of a beam in the 1st example is $L = 300$ cm, while in the 2nd example a length $L = 1200$ cm is chosen. The typical kinematic quantities of the beam from 1st example are presented in Figs. 4–6 in the columns on the left, while the quantities from 2nd example are presented in the columns on the right. For each example
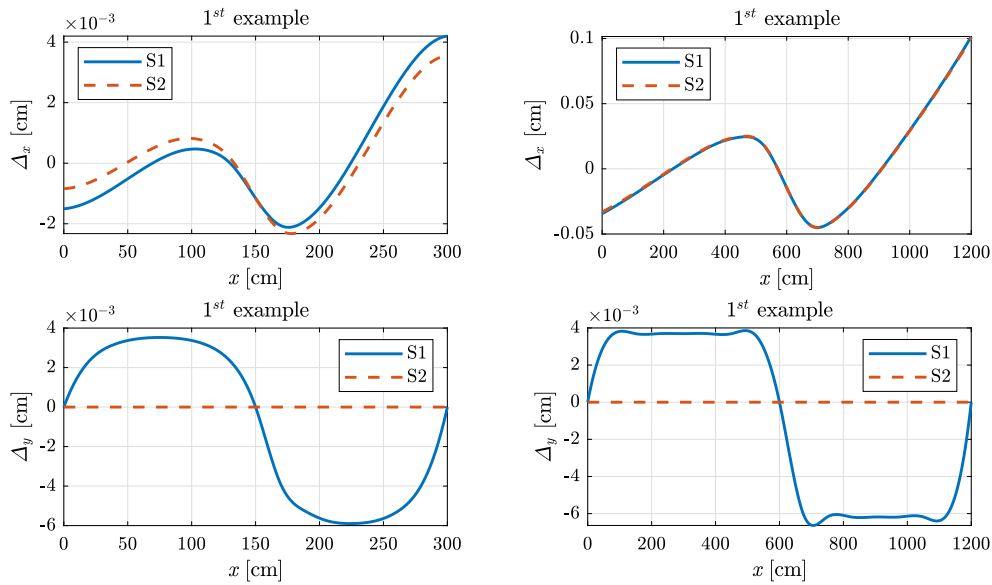
Fig. 4. Inter-layer slip Δ_x and Δ_y for the 1st example (left column) and the 2nd example (right column).
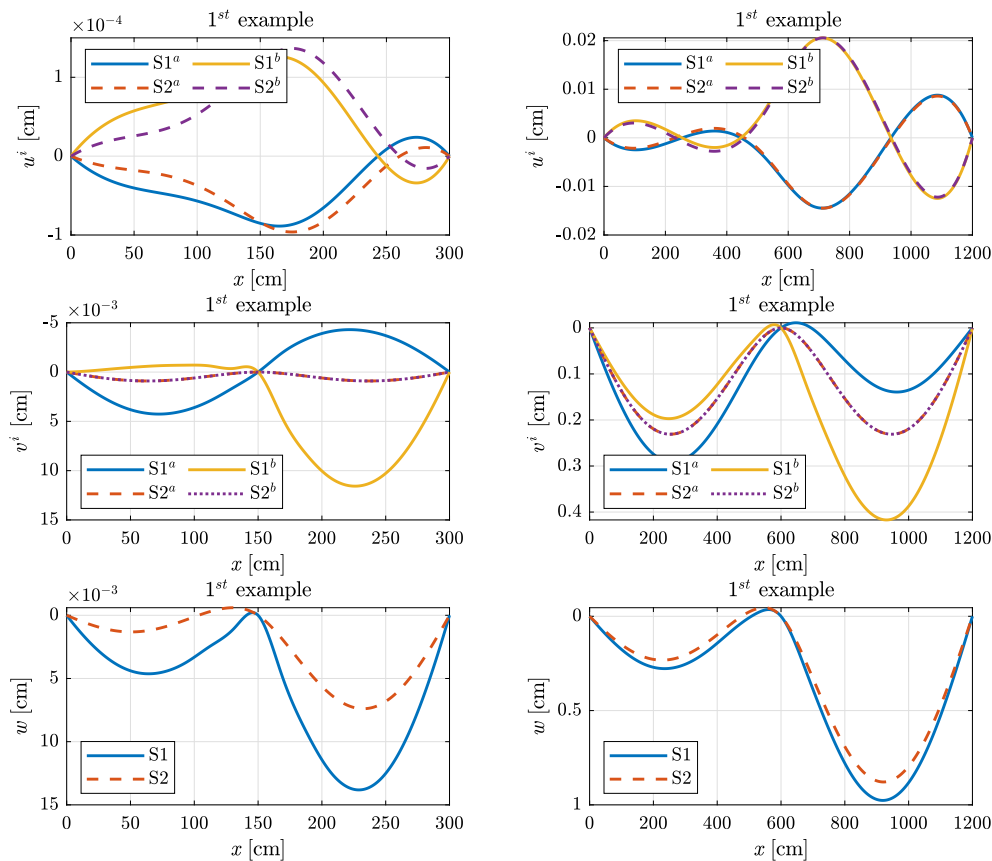

Fig. 5. Displacements u^i, v^i and w for the 1st example (left column) and the 2nd example (right column).

two parametric studies have been made. In the 1st study, named S1, the shear stiffness $G^i A_s^i$ of each layer of the beam is the same as the one in illustrative example, while in the 2nd study, named S2, we multiply it by 10^8. With this greatly exaggerated shear stiffness, cross-sectional shear deformations are practically prevented. Now the effect of shear stiffness on typical quantities in beams with different lengths can be analysed. Where quantities of different layers are presented, we name them as S1^i or S2^i, where $i = a, b$. Static quantities are not presented, since they reflect the behaviour of already discussed kinematic quantities.

In Fig. 4 one can see that cross-sectional shear stiffness has great effect on longitudinal inter-layer slip Δ_x when dealing with short beams,
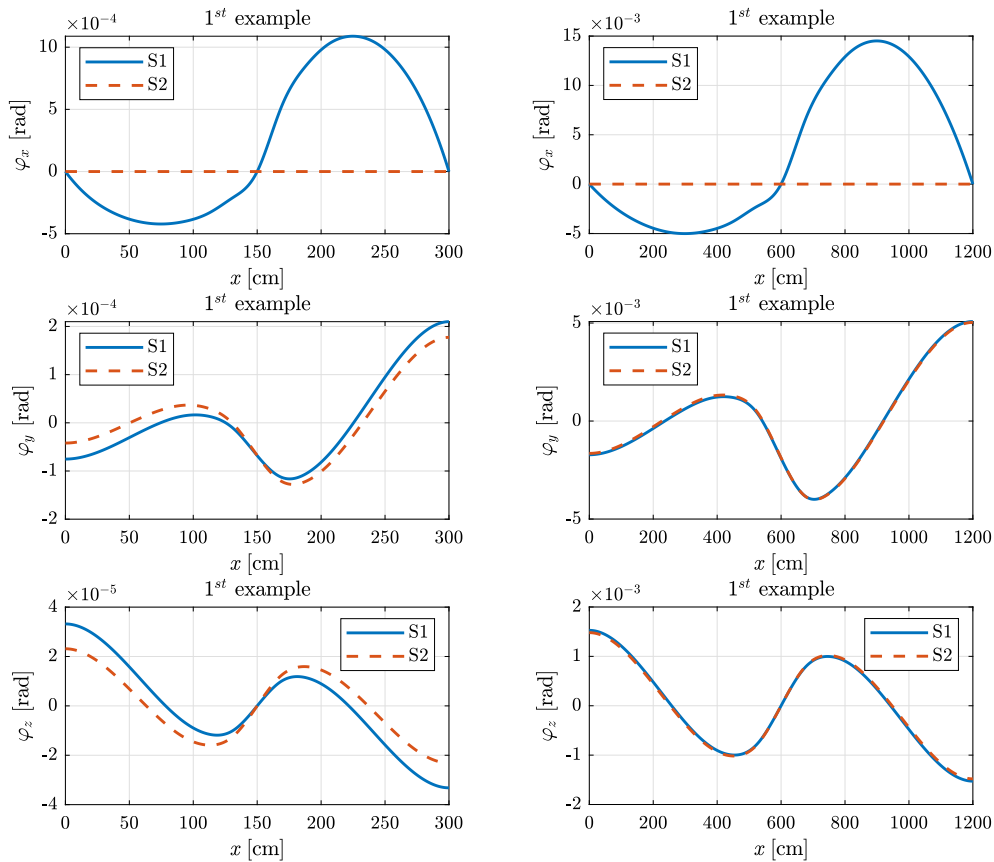
Fig. 6. Rotations φ_x, φ_y and φ_z for the 1st example (left column) and the 2nd example (right column).

whereas with longer beams, this effect is negligible. When looking at transverse inter-layer slip Δ_y, both short and long beam experience zero transverse inter-layer slip in S2 study, while it varies with length in S1 study. This is due to the constraining Eqs. (9), where longitudinal inter-layer slip Δ_x is dependant on longitudinal displacements u^a and u^b and on bending rotation φ_y, while transverse inter-layer slip Δ_y is dependant on transverse displacements v^a and v^b and on torsional rotation φ_x. If shear stiffness of layer a and b is big (case S2), the torsional rotation φ_x will be close to zero and both transverse displacements v^a and v^b will be practically the same. Consequently, transverse inter-layer slip will be close to zero, regardless of the beam length. The same cannot be said for longitudinal inter-layer slip Δ_x, since bending rotation φ_y is mostly dependant on bending stiffness of the beam and not so much on shear stiffness itself. Hence, only smaller or bigger inter-layer slip will occur in cases where shear stiffness has influence, *i.e.* in beams with short spans, while in beams with longer spans, the shear stiffness is neglected and inter-layer slip Δ_x is practically independent of it. The same phenomenon can be observed with other kinematic quantities presented in Figs. 5 and 6. When dealing with short beams, the shear cross-sectional stiffness has big effect on longitudinal displacements u^i, vertical displacement w and both of the bending rotations φ_y and φ_z. On the other hand, when dealing with longer beams, the effect can be practically neglected. When looking at torsional rotation φ_x, one can see, that length of the beam has no effect on the course of the line, since torsional rotation in beam with cross-section rigid in shear is practically negligible regardless of the length of the beam. Based on the results from Figs. 4–6 one can conclude that shear cross-sectional stiffness has big effect on shorter beams, while in longer beams the effect can be negligible. The displacements and rotations of the beam depend both on bending and on shear stiffness of the beam. With longer beams the bending stiffness is a lot smaller then with shorter beams, while shear

Table 4
Contact stiffnesses for each calculation.

	K_x [kN/cm]	K_y [kN/cm]
V1	10^{-8}	10^{-8}
V2	10	10
V3	10^8	10^8

stiffness does not change that much, thus displacements and rotations in longer beams are mainly because of the bending part.

4.3. Parametric study of the effect of contact stiffness

Contact stiffness K_x and K_y can also greatly influence the behaviour of composite beam. In this subsection a beam from illustrative example with a length of $L = 600$ cm is used, where three different calculations, each with different contact stiffness, are carried out. Contact stiffnesses for each calculation are shown in Table 4.

In this study only kinematic quantities of the beam are presented, since they already fully present the effect of contact stiffness on the behaviour of the beam. In example V1, the contact stiffness is already so small, that there is practically no connection between the layers, while in example V3, the contact stiffness is so big, that the contact is practically rigid.

By looking at Figs. 7 and 8, one can see that contact stiffness greatly influence the behaviour of a composite beam. If the contact is rigid, the composite beam, made of two layers, acts as one beam without layers and consequently rotations and displacements are smaller, since the beam is stiffer. Similarly, if the contact stiffness is close to zero, the two layers act on its own almost like two separate beams, thus the stiffness is smaller and displacements and rotations are bigger.
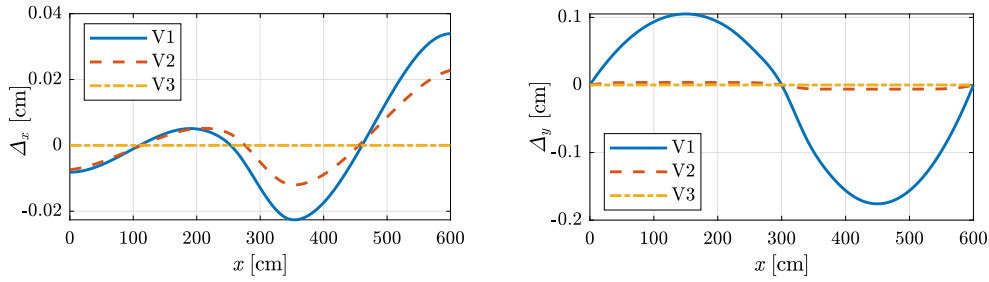
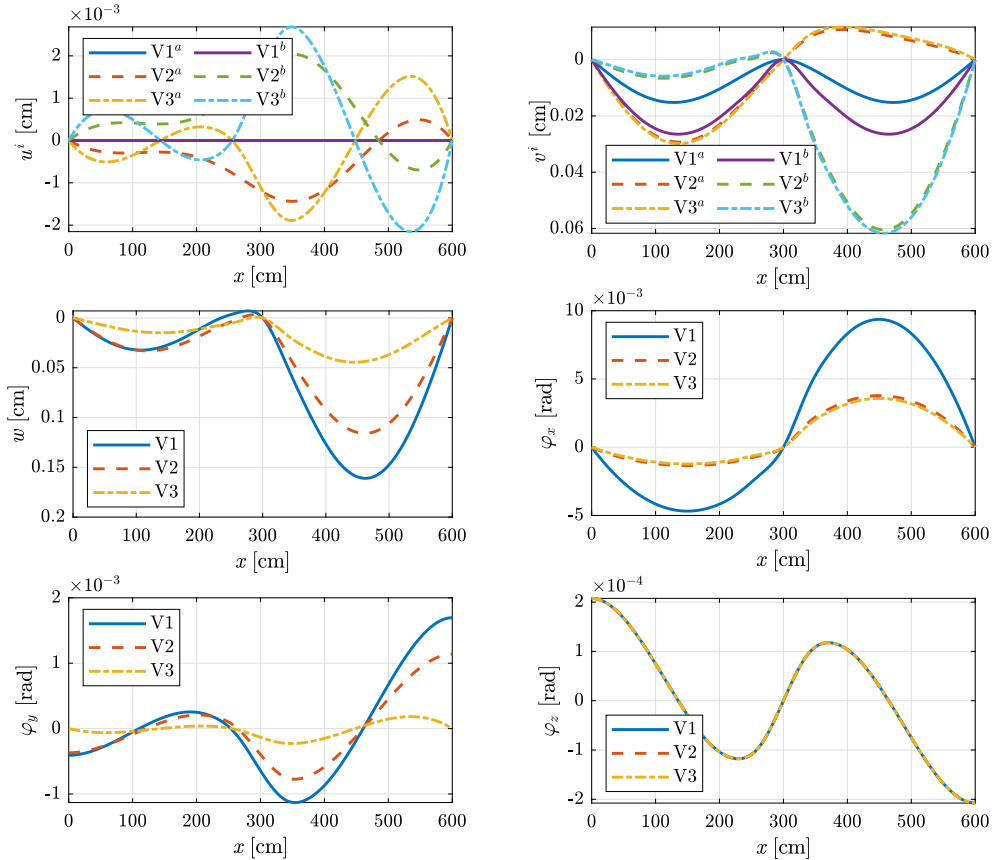**Fig. 7.** Inter-layer slips, Δ_x and Δ_y, for each of the calculations V1–V3.

Fig. 8. Displacements and rotations of the beam for each of the calculations V1–V3.

4.4. Parametric study of the effect of both cross-sectional shear stiffness and contact stiffness

By combining parametric studies from Sections 4.2 and 4.3, one can observe the behaviour of a beam when length L, longitudinal and transverse contact stiffness K_x and K_y and cross-sectional shear stiffness for each layer $G^i A_s^i$ are varied. In this parametric study, a vertical displacement, w, and both transverse displacements, v^a and v^b, at $x = 3L/4$ are observed. Vertical displacements with cross-sectional shear stiffness being the same as in illustrative example are denoted as w_1, while vertical displacements with practically rigid cross-sectional stiffness (i.e. with cross-sectional stiffness multiplied by 10^8) are denoted as w_2. Similarly, the transverse displacements v^a and v^b is named as v_1^a, v_1^b and v_2^a, v_2^b. Results are presented in Fig. 9, where horizontal axis represents a fracture between the height of the beam $h = h^a + h^b$ and length of the beam L and vertical axis represents a fracture between w_1, v_1^a, v_1^b and w_2, v_2^a, v_2^b.

Fig. 9 clearly shows that with the increase of the factor h/L, the relation between w_1, v_1^a, v_1^b and w_2, v_2^a, v_2^b always goes towards value

one, regardless of contact stiffness. There have been none numerical problems with any combination of length and stiffness in this study. Thus, we have proven that shear locking is not an issue with the presented type of finite element.

5. Conclusions

The paper presents a new mathematical and numerical model for the analysis of the two-layer spatial beams with inter-layered slip in longitudinal and transverse direction and with shear deformations taken into account. To avoid negative effects of poorly conditioned equations due to the constraining equations, one can consistently separate the equations into two unrelated groups which is an important advantage over commercial software. The equations are then solved numerically, by using a new family of deformation based finite elements, where deformations are interpolated by using Lagrange polynomials. By doing that, one can avoid all kinds of locking. This statement is supported also by having no numerical problems during parametric studies presented herein. In fact, the parametric study in Section 4.4
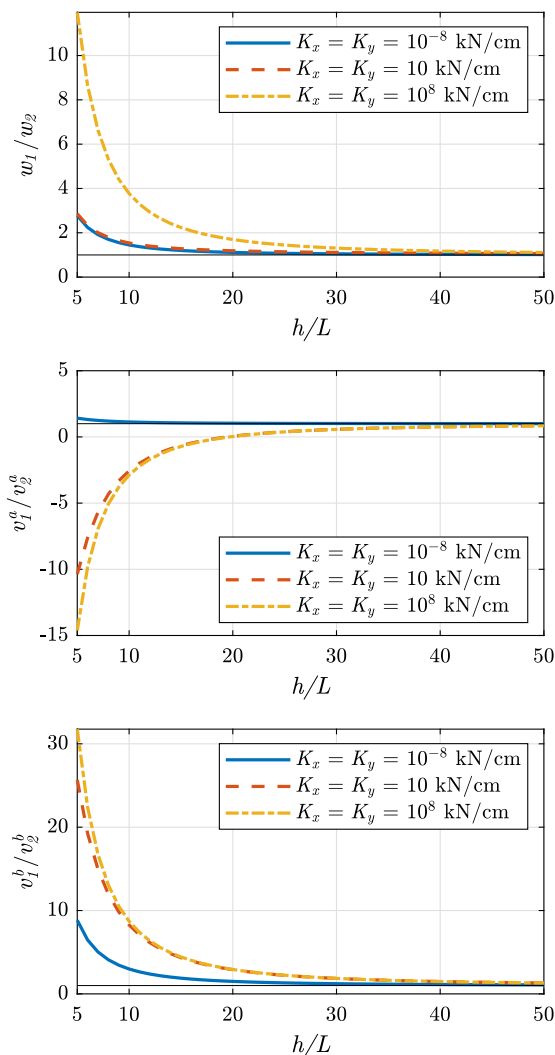
Fig. 9. Parametric study of vertical displacement, w, and transverse displacements, v^a and v^b, with length L, contact stiffness K_x and K_y and cross-sectional stiffness $G^i A_s^i$ varied.

has been designed in a way to trigger numerical problems if they were to occur, which they did not.

A convergence study has shown a great accuracy of such finite elements, since 4 finite elements type FE_{3-4} or 16 finite elements type FE_{1-2} already give almost exact values of typical physical quantities. In the illustrative example a timber two-layer T-shaped beam was presented. Beam was loaded with various different external line loads by which we showed the spatial response. One of the most important findings in the paper is that one should always consider real shear cross-sectional stiffness of the beam, since the behaviour of the beam is very much dependent on it. It is also very important to consider contact stiffness between layers accordingly, when one designs composite beams, since the contact stiffness can greatly influence the behaviour of the composite beam.

The presented model for two-layered composite beam can already be applied to various different cases, since each of the layer can be made of different linear material and contact behaviour can be defined with adequate linear contact stiffness. For example, a steel–concrete, timber–concrete or timber–timber composite beam can be analysed, where one can use various different types of shear connections (shear studs, adhesive in glued joints, bolts or nails in tension or shear, *etc.*) with previously determined contact stiffness. Since the range of the contact stiffness in the model is not limited, one can successfully analyse

composite beams with full shear connection, partial shear connection or even zero shear connection between layers. The model however is currently limited to linear elastic response and thus, in order to obtain valid results, the applied external load range should be sufficiently small.

In further research, the presented linear elastic model of the composite beam will be upgraded with a nonlinear one and also fire analysis of the composite beam will be added. Nowadays researchers mostly focus on nano research, such as research in porous beams and plates [62–69], however an extensive research remains to be done on spatial composite beams, such as nonlinear spatial behaviour of composite beams exposed to fire.

Declaration of competing interest

The authors declare that they have no known competing financial interests or personal relationships that could have appeared to influence the work reported in this paper.

Acknowledgments

References

[1] Richard Liew JY, Sohel KMA, Koh CG. Impact tests on steel–concrete–steel sandwich beams with lightweight concrete core. Eng Struct 2009;31:2045–59.

[2] Liew JYR, Yan LB, Huang ZY. Steel–concrete–steel sandwich composite structures-recent innovations. J Constr Steel Res 2017;130:202–21.

[3] Yeoh D, Fragiacomo M, Franceschi M, Boon KH. State of the art on timber–concrete composite structures: Literature review. J Struct Eng 2011;137(10):1085–95.

[4] Hozjan T, Saje M, Srpčič S, Planinc I. Geometrically and materially non-linear analysis of planar composite structures with an interlayer slip. Comput Struct 2013;114–115:1–17.

[5] Newmark NM, Siest CP, Viest CP. Test and analysis of composite beams with incomplete interaction. Proc Soc Exp Stress Anal 1951;1:75–92.

[6] Goodman JR, Popov EP. Layered beam systems with interlayer slip. J Struct Div 1968;94(11):2535–48.

[7] Goodman JR, Popov EP. Layered wood systems with inter-layer slip. Wood Sci 1969;1(3):148–58.

[8] Girhammar UA, Gopu VKA. Composite beam-columns with inter-layer slip-exact analysis. J Struct Eng ASCE 1993;199(4):1265–82.

[9] Girhammar UA. A simplified analysis method for composite beams with interlayer slip. Int J Mech Sci 2009;51:515–30.

[10] Focacci F, Foraboschi P, Stefano M. Composite beam generally connected: Analytical model. Compos Struct 2015;133:1237–48.

[11] Schnabl S, Planinc I, Saje M, Čas B, Turk G. An analytical model of layered continuous beams with partial interaction. Struct Eng Mech 2006;22(3):263–78.

[12] Sousa Jr JBM, Silva AR. Analytical and numerical analysis of multilayered beams with interlayer slip. Eng Struct 2010;32:1671–80.

[13] Škec L, Schnabl S, Planinc I, Jelenić G. Analytical modelling of multilayer beams with compliant interfaces. Struct Eng Mech 2012;44(4):465–85.

[14] Monetto I. Analytical solutions of three-layer beams with interlayer slip and step-wise linear interface law. Compos Struct 2015;120:543–51.

[15] Foraboschi P. Three-layered sandwich plate: Exact mathematical model. Composites B 2013;45:1601–12.

[16] Foraboschi P. Three-layered plate: Elasticity solution. Composites B 2014;60:764–76.

[17] Wu P, Zhou D, Liu W. 2-D elasticity solutions of two-layer composite beams with an arbitrarily shaped interface. Appl Math Model 2016;40(2):1477–93.

[18] Schnabl S, Saje M, Turk G, Planinc I. Analytical solution of two-layer beam taking into account interlayer slip and shear deformation. J Struct Eng ASCE 2007;133(6):886–94.

[19] Ecsedi I, Baksa A. Analytical solution for layered composite beams with partial shear interaction based on Timoshenko beam theory. Eng Struct 2016;115:107–17.

[20] Kroflič A, Planinc I, Saje M, Čas B. Analytical solution of two-layer beam including interlayer slip and uplift. Struct Eng Mech 2010;34(6):667–83.

[21] Schnabl S, Planinc I. Exact buckling loads of two-layer composite Reissner's columns with interlayer slip and uplift. Int J Solids Struct 2013;50:30–7.

[22] Foraboschi P. Analytical solution of two-layer beam taking into account nonlinear interlayer slip. J Eng Mech 2009;135(10):1129–46.

[23] Campi F, Monetto I. Analytical solutions of two-layer beams with interlayer slip and bi-linear interface law. Int J Solids Struct 2013;50:687–98.

[24] Schnabl S, Jelenić G, Planinc I. Analytical buckling of slender circular concrete-filled steel tubular columns with compliant interfaces. J Constr Steel Res 2015;115:252–62.

[25] Girhammar UA, Pan DH, Gustafsson A. Exact dynamic analysis of composite beams with partial interaction. Int J Mech Sci 2009;51:565–82.

[26] Fabbrocino G, Manfredi G, Cosenza E. Non-linear analysis of composite beams under positive bending. Comput Struct 1999;70:77–89.

[27] Čas B. Nonlinear analysis of composite beams with inter-layer slip taken into account (Ph.D. thesis), Ljubljana: University of Ljubljana, Faculty of Civil and Geodetic Engineering; 2004 [in Slovene].

[28] Faella C, Martinelli E, Nigro E. Steel-concrete composite beams in partial interaction: Closed-form "exact" expression of the stiffness matrix and the vector of equivalent nodal forces. Eng Struct 2010;32(9):2744–54.

[29] Kroflič A, Saje M, Planinc I. Non-linear analysis of two-layer beams with interlayer slip and uplift. Comput Struct 2011;89(23-24):2414–24.

[30] Chakrabarti A, Sheikh AH, Griffith M, Oehlers DJ. Analysis of composite beams with partial shear interactions using a higher order beam theory. Eng Struct 2012;36:283–91.

[31] Kroflič A. Non-linear analysis of multilayer composite structures (Ph.D. thesis), Ljubljana: University of Ljubljana, Faculty of Civil and Geodetic Engineering; 2012 [in Slovene].

[32] Sousa Jr JBM. Exact finite elements for multilayered composite beam-columns with partial interaction. Comput Struct 2013;123:48–57.

[33] Nguyen QH, Hjiaj M, Lai VA. Force-based FE for large displacement in elastic analysis of two-layer Timoshenko beams with interlayer slips. Finite Elem Anal Des 2014;85:1–10.

[34] Lo SH, Li L, Su RKL. Optimization of partial interaction in bolted side-plated reinforced concrete beams. Comput Struct 2014;131:70–80.

[35] Xu R, Wu YF. Free vibration and buckling of composite beams with interlayer slip by two-dimensional theory. J Sound Vib 2008;313(3-5):875–90.

[36] Shen X, Chen W, Wu Y, Xu R. Dynamic analysis of partial-interaction composite beams. Compos Sci Technol 2011;71:1286–94.

[37] Lenci S, Clementi F. Effects of shear stiffness, rotatory and axial inertia, and interface stiffness on free vibrations of a two-layer beam. J Sound Vib 2012;331:5247–67.

[38] Schnabl S, Planinc I, Turk G, Srpčič S. Fire analysis of timber composite beams with interlayer slip. Fire Saf J 2009;44(5):770–8.

[39] Hozjan T. Nonlinear analysis of composite planar structures exposed to fire (Ph.D. thesis), Ljubljana: University of Ljubljana, Faculty of Civil and Geodetic Engineering; 2009 [in Slovene].

[40] Hozjan T, Saje M, Srpčič S, Planinc I. Fire analysis of steel–concrete composite beam with interlayer slip. Comput Struct 2011;89:189–200.

[41] Kolšek J, Saje M, Planinc I, Hozjan T. A fully generalised approach to modelling fire response of steel–RC composite structures. Int J Non-Linear Mech 2014;67:382–93.

[42] Challamel N, Girhammar UA. Lateral-torsional buckling of partially composite horizontally layered or sandwich-type beams under uniform moment. J Eng Mech 2013;139:1047–64.

[43] Čas B, Planinc I, Schnabl S. Analytical solution of three-dimensional two-layer composite beam with interlayer slips. Eng Struct 2018;173:269–82.

[44] Udovč G, Planinc I, Hozjan T. Analysis of two-layer spatial composite beams taking into account shear deformations and longitudinal inter-layer slip. In: Kuhljevi dnevi 2021. 2021, p. 209–18 [in Slovene].

[45] Udovč G, Hozjan T, Planinc I, Ogrin A. Analysis of two-layer spatial beams with inter-layer slip. Gradbeni vestnik 2022;71:201–22 [in Slovene].

[46] Simo JC. A finite strain beam formulation. The three-dimensional dynamic problem. Part I. Comput Methods Appl Mech Engrg 1985;49:55–70.

[47] Taylor RL, Filippou FC, Saritas A, Auricchio F. A mixed finite element method for beam and frame problems. Comput Mech 2003;31:192–203.

[48] Hughes TJR, Taylor RL, Kanoknukulchai W. A simple and efficient finite element for plate bending. Internat J Numer Methods Engrg 1977;11:1529–43.

[49] Rezaiee-Pajand M, Gharaei-Moghaddam N. Analysis of 3D Timoshenko frames having geometrical and material nonlinearities. Int J Mech Sci 2015;94–95:140–55.

[50] Rezaiee-Pajand M, Gharaei-Moghaddam N. Frame nonlinear analysis by force method. Int J Steel Struct 2017;17(2):609–29.

[51] Kusuma Chandrashekhara S, Zupan D. Path following using velocity-based approach in quasi-static analysis. Int J Solids Struct 2023;275:1–15.

[52] Soydas O, Saritas A. An accurate nonlinear 3D Timoshenko beam element based on hu-washizu functional. Int J Mech Sci 2013;74:1–14.

[53] Soydas O, Saritas A. Free vibration characteristics of a 3D mixed formulation beam element with force-based consistent mass matrix. J Vib Control 2015;23(16):1–21.

[54] Saje M, Planinc I, Turk G, Vratanar B. A kinematically exact finite element formulation of planar elastic-plastic frames. Comput Methods Appl Mech Engrg 1997;144:125–51.

[55] Saje M, Turk G, Kalagasidu A, Vratanar B. A kinematically exact finite element formulation of elastic-plastic curved beams. Comput Struct 1998;67:197–214.

[56] Choi J, Lim J. General curved beam elements based on the assumed strain fields. Comput Struct 1995;55:379–86.

[57] Hjelmstad KD. Fundamentals of structural mechanics. Second Edition. Illinois: Springer; 2005.

[58] Cowper GR. The shear coefficient in Timoshenko's beam theory. J Appl Mech 1966;33(2):335–40.

[59] Huang Z, Burgess IW, Plank RJ. The influence of shear connectors on the behaviour of composite steel-framed buildings in fire. J Constr Steel Res 1999;51:219–37.

[60] Eurocode 5: Design of timber structures - Part 1-1: General-common rules and rules for buildings. Tech. Rep. European committee for standardization, Brussels, BE.

[61] Planinc I. A quadratically convergent algorithms for the computation of stability points (Ph.D. thesis), Ljubljana: University of Ljubljana, Faculty of Civil and Geodetic Engineering; 1998 [in Slovene].

[62] Alimirzaei S, Mohammadimehr M, Tounsi A. Nonlinear analysis of viscoelastic micro-composite beam with geometrical imperfection using FEM: MSGT electro-magneto-elastic bending, buckling and vibration solutions. Struct Eng Mech 2019;71(5):485–502.

[63] Kumar Y, Gupta A, Tounsi A. Size-dependent vibration response of porous graded nanostructure with FEM and nonlocal continuum model. Adv Nano Res 2021;11(1):1–17.

[64] Cuong LT, Minh HL, Nguyen PT, Phan-Vu P. Nonlinear bending analysis of porous sigmoid FGM nanoplate via IGA and nonlocal strain gradient theory. Adv Nano Res 2022;12(5):441–55.

[65] Garg A, Belarbi MO, Tounsi A, Li L, Singh A, Mukhopadhyay T. Predicting elemental stiffness matrix of FG nanoplates using Gaussian process regression based surrogate model in framework of layerwise model. Eng Anal Bound Elem 2022;143:779–95.

[66] Vinh PV, Chinh NV, Tounsi A. Static bending and buckling analysis of bi-directional functionally graded porous plates using an improved first-order shear deformation theory and FEM. Eur J Mech A Solids 2022;96:104743.

[67] Katiyar V, Gupta A, Tounsi A. Microstructural/geometric imperfection sensitivity on the vibration response of geometrically discontinuous bi-directional functionally graded plates (2DFGPs) with partial supports by using FEM. Steel Compos Struct 2022;45(5):621–40.

[68] Xia L, Wang R, Chen G, Asemi K, Tounsi A. The finite element method for dynamics of FG porous truncated conical panels reinforced with graphene platelets based on the 3-D elasticity. Adv Nano Res 2023;14(4):375–89.

[69] Mesbah A, Belabed Z, Amara K, Tounsi A, Bousahla AA, Bourada F. Formulation and evaluation a finite element model for free vibration and buckling behaviours of functionally graded porous (FGP) beams. Struct Eng Mech 2023;86(3):291–309.